# A two-in-one molybdenum disulfide-chitosan nanoparticles system for activating plant defense mechanisms and reactive oxygen species to treat *Citrus* Huanglongbing

Guiyun Deng [a,1], Feifan Lu [a,1], Shuojun Li [a,c,1], Yuying Long [a], Jianghong Wu [a], Xiaofeng Guo [a], Chunyin Li [a], Zhiyong Song [a], Mohamed F. Foda [d,e], Fang Ding [b,*], Heyou Han [a,*]

[a] *National Key Laboratory of Agricultural Microbiology, College of Life Science and Technology, Huazhong Agricultural University, Wuhan, Hubei 430070, China*
[b] *Hubei Key Laboratory of Plant Pathology, College of Plant Science and Technology, Huazhong Agricultural University, Wuhan, Hubei 430070, China*
[c] *National Key Laboratory of Molecular Biology, CAS Center for Excellence in Molecular Cell Science, Shanghai Institute of Biochemistry and Cell Biology, 200031, China*
[d] *National Key Laboratory of Crop Genetic Improvement, College of Life Science and Technology, Huazhong Agricultural University, Wuhan 430070, China*
[e] *Department of Biochemistry, Faculty of Agriculture, Benha University, Moshtohor, Toukh 13736, Egypt*

## ARTICLE INFO

## ABSTRACT

*Citrus* Huanglongbing (HLB) poses an enormous challenge to *Citrus* cultivation worldwide, necessitating groundbreaking interventions beyond conventional pharmaceutical methods. In this study, we propose molybdenum disulfide-chitosan nanoparticles (MoS$_2$-CS NPs) through electrostatic adsorption, preserving the plant-beneficial properties of molybdenum disulfide (MoS$_2$), while enhancing its antibacterial effectiveness through chitosan modification. MoS$_2$-CS NPs exhibited significant antibacterial efficacy against *RM1021*, and the closest relatives to *Candidatus* Liberibacter asiaticus (*C*Las), *Erwinia carotovora*, and *Xanthomonas citri* achieved survival rates of 7.40 % ± 1.74 %, 8.94 % ± 1.40 %, and 6.41 % ± 0.56 %, respectively. *In vivo* results showed, *C*Las survival rate of 10.42 % ± 3.51 %. Furthermore, treatment with MoS$_2$-CS NPs resulted in an increase in chlorophyll and carotenoid content. Concomitantly, a significant reduction in malondialdehyde (MDA), soluble sugar, hydrogen peroxide (H$_2$O$_2$), and starch contents was also observed. Mechanistically, MoS$_2$-CS NPs enhanced the activity of antioxidant-related enzymes by upregulating the expression of antioxidant genes, thereby galvanizing the antioxidant system to alleviate oxidative stress. Collectively, this dual functionality—combining direct antibacterial action with the activation of plant defense mechanisms—marks a promising strategy for managing *Citrus* Huanglongbing and suggests potential agricultural applications for MoS$_2$-based antibacterial treatments.

## 1. Introduction

*Citrus*, one of the world's top three fruit crops, is vital to global agriculture, offering various health benefits, including a rich supply of vitamin C. However, the *Citrus* industry faces severe economic challenges owing to *Citrus* Huanglongbing (HLB), a devastating disease often referred to as "orange cancer" [1]. This disease is caused by the *α-Proteobacteria Candidatus Liberibacter spp.*, which is mainly divided into *Ca. L. asiaticus* (*C*Las), *Ca. L. americanus* (*C*Lam) and *Ca. L. africanus* (*C*Laf), among which *C*Las is the most predominant and prevalent strain [2]. The virulence of HLB disease is evident in symptoms such as yellow-mottled leaves, fruit drop, and root decay, which ultimately threaten the livelihood of farmers [3]. The phloem-limited nature of *C*Las coupled with its resistance to *in vitro* culture makes the development of effective treatments particularly challenging [4]. Traditional methods to control plant diseases, including the use of antibiotics, cut down diseased trees, or inhibit the propagation of psyllid to cut off the transmission route of HLB, that have led to the emergence of drug-resistant strains and causing huge economic losses (Schema 1), Antibiotics' extensive use in agriculture to boost crop growth and prevent diseases has fostered the emergence of antibiotic-resistant plant pathogens, threatening both agricultural productivity and food safety [5]. Additionally, residues from these antibiotics in foodstuffs can fuel resistance in human and animal pathogens, risking public health. The

prevalence of antibiotic-resistant bacteria in livestock, a key source of foodborne illnesses, further escalates this risk, undermining antibiotic treatments and raising concerns over disease management and associated health outcomes [6]. Although the antibacterial and antimicrobial properties of various nanoparticles have been studied, especially concerning HLB [8–10], there is a need for novel solutions that offer comprehensive disease management.

Compared to conventional materials, nanomaterials exhibit unique physical and chemical properties due to their small particle size and large surface area to volume ratio, which are not observed in traditional materials. Consequently, nanomaterials have been utilized as carriers, with metal nanoparticles (such as inorganic nanomaterials, gold nanoparticles) and bioactive nanoparticles (such as nano-hydroxyapatite, carbon nanotubes) serving as nanocarriers in the controlled and targeted release of agrochemicals and fertilizers. Natural polymers like chitosan and alginate, while synthetic polymers such as polylactic acid (PLA), polyethylene glycol (PEG), and polycaprolactone (PCL) can be engineered for specific Polymeric nanoparticles [7]. However, the distinctive characteristics of nanomaterials may also engender adverse effects on human health and the ecological environment. Studies have indicated that the primary factors contributing to the toxicity of nanomaterials are their inherent physicochemical properties and environmental conditions, such as particle size, concentration, exposure duration, temperature, and ultraviolet radiation, all of which can influence the degree of toxicity exhibited by nanomaterials. [8–10]. ROS, including singlet oxygen, peroxides, and hydroxyl radicals, exert significant oxidative stress on biological and synthetic substrates through free radical reactions. Antioxidants are crucial for countering these oxidative challenges. Nature has endowed organisms with a repertoire of antioxidants; humans with vitamins [11] and plants with lignin [12], to maintain redox homeostasis. The biocompatibility of these natural antioxidants is highly prized in medical applications. Despite their promise, bio-based antioxidants face degradation by microorganisms and reduced effectiveness outside their physiological context, limiting their utility in agriculture [13]. To bolster lignin's antioxidant resilience, researchers have investigated all-biomass membranes. Concurrently, the development of xylose-based hemicellulose nanocrystals has emerged as a strategy to improve lignin's stability in aqueous environments, thereby amplifying its antioxidant potential [14,15].

Among these, molybdenum disulfide nanoparticles ($MoS_2$ NPs), a type of two-dimensional nanomaterial, have gained attention for their diverse applications, including antibacterial activities, drug delivery, phototherapy, biosensing, water disinfection, antibacterial wound healing, and oncology [16–19]. $MoS_2$ NPs have demonstrated efficacy in animal models by disrupting bacterial membranes, perturbing bacterial metabolism, and inducing reactive oxygen species (ROS) with minimal toxicity to mammalian cells [20,21]. Their potential in agriculture, particularly in promoting plant growth and activating antioxidant systems, has also been explored [22,23]. Additionally, $MoS_2$ itself exhibits antioxidant-like enzymatic attributes to mitigate plant oxidative stress [24]. These multifaceted traits render $MoS_2$ a promising candidate for mitigating HLB-associated pathologies, including ROS accumulation, chlorophyll deficiency, and micronutrient [25–27]. However, despite their promising attributes, the application of $MoS_2$ in plant disease resistance, particularly against HLB, has not been fully realized [28,29]. The present pharmacological arsenal against HLB encompasses antibacterial peptides [30], oak extracts [31], nanosilver [32], and the symptom-alleviating antioxidant gibberellin [25,32].

This study aims to bridge this gap by introducing a bifunctional approach employing $MoS_2$-chitosan nanoparticles ($MoS_2$-CS NPs) to target HLB. Unlike previous studies that primarily focused on antibacterial activities, this study emphasizes the dual-action capability of
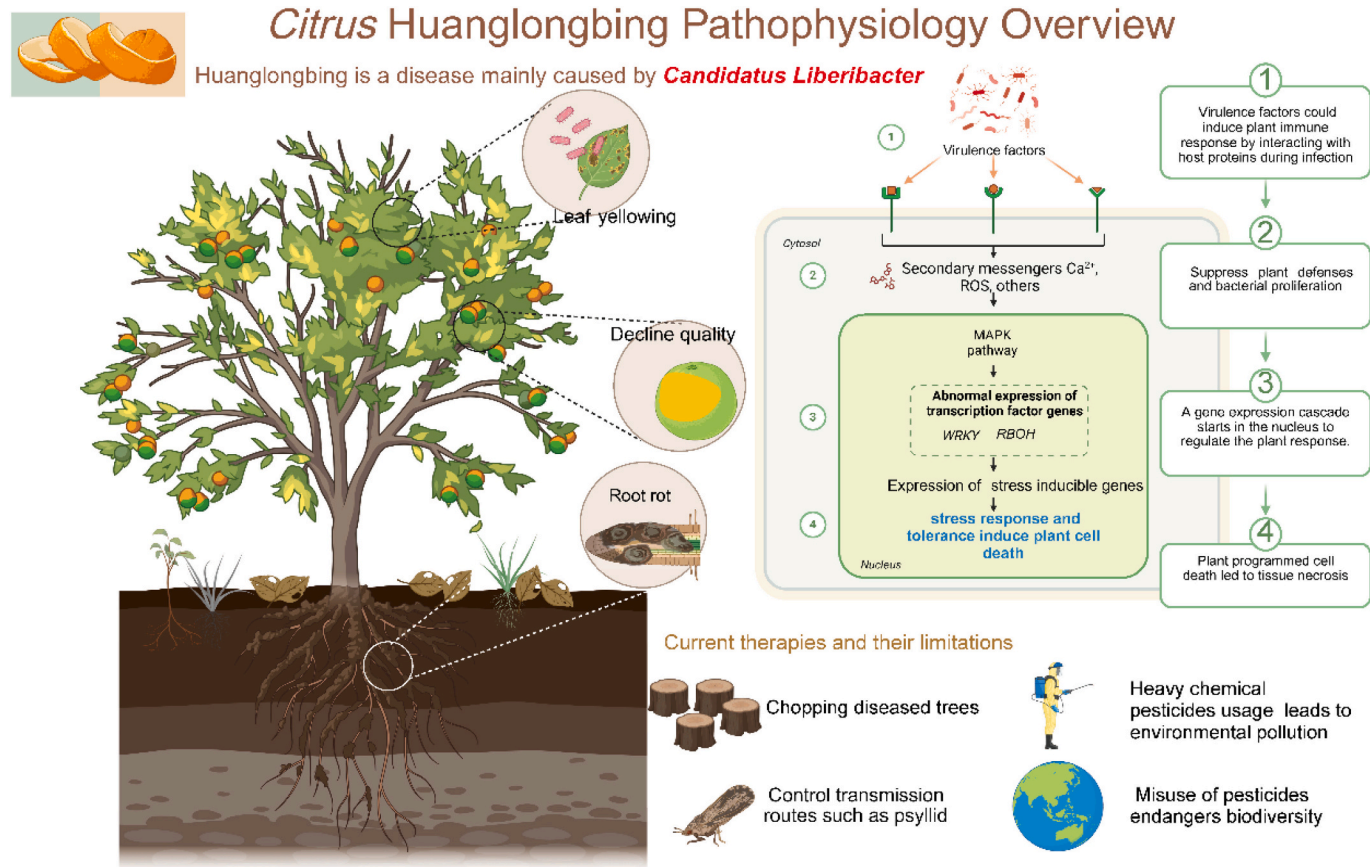


**Schema 1.** *Citrus* Huanglongbing pathophysiology, including molecular mechanisms, most relevant pathogens, and current therapies and their limitations.

MoS$_2$-CS NPs: inhibiting *C*Las proliferation while simultaneously alleviating *C*Las-induced oxidative stress. Chitosan is an excellent choice for the surface modification of MoS$_2$ NPs due to its biocompatibility, biodegradability, permeability, cost-effectiveness, low toxicity, and environmental friendliness [33]. By integrating the biocompatible and antibacterial properties [34] of chitosan with the inherent plant growth-promoting, enhancing chlorophyll content, displaying antibacterial potency against *C*Las, and circumventing the constraints of near-infrared (NIR) stimulation and antioxidant-activating characteristics of MoS$_2$, this study presents a novel and comprehensive strategy for managing *Citrus* HLB. Interestingly, MoS$_2$-CS NPs exhibited potent *in vitro* and *in vivo* antibacterial efficacy against *RM1021, Erwinia carotovora, Xanthomonas citri,* and *C*Las, eliciting the upregulation of defense marker genes to bolster HLB resistance and antioxidant-related genes to activate the plant antioxidant system. These results indicate that MoS$_2$-CS NPs are a promising comprehensive intervention strategy for the integrated control of *Citrus* HLB.

## 2. Materials and experiment

### 2.1. Materials

Bulk MoS$_2$, chitosan (No carboxylation, low viscosity, <200 mPa.s), iodine, trichloroacetic acid, and thiobarbituric acid were purchased from Aladdin Industrial Corporation (Shanghai, China). Ethanol, acetic acid, soluble starch, ascorbic acid, hydrogen peroxide, calcium nitrate, sodium hydroxide, hydrochloric acid, Sager-Granick medium, and Nutrient Agar were obtained from Sinopharm Chemical Reagent (Shanghai, China). Plant materials were 1-year old HLB-positive and healthy Valencia sweet orange (*Citrus sinensis*) plants were maintained in a greenhouse (27 ± 2 °C, relative humidity of 50 ± 5 %, and natural light period). *Citrus* trees infected with Huanglongbing came from Guangxi Characteristic Crop Research Institute. *RM1021, Erwinia carotovora*, and *Xanthomonas citri* came from the conservation of the College of Plant Science and Technology of Huazhong Agricultural University.

### 2.2. Synthesis of MoS$_2$-CS NPs

MoS$_2$-CS NPs were synthesized by ultrasonic exfoliation of bulk MoS$_2$ in the aqueous phase, and the subsequent MoS$_2$-CS NPs by electrostatic adsorption with CS acetic acid solution. In brief, 200 mg of bulk MoS$_2$ was first dispersed in deionized water for bath sonication for 5 min and then exfoliated by probe sonication for 2 h with a 3 s on/off cycle. After the completion of exfoliation, the MoS$_2$ NPs were obtained in the supernatant, while the bulk MoS$_2$ was recycled at the bottom by centrifugation at 4500 rpm. Subsequently, the MoS$_2$ NPs were added to the CS acetic acid solution (60 mg chitosan in 12 mL 0.2 % acetic acid solution) with centrifugation at 12000 rpm after 2 h of stirring, and the precipitate was washed three times using deionized water. Finally, MoS$_2$-CS NPs were obtained by freeze-drying.

### 2.3. Characterization

Bulk MoS$_2$, MoS$_2$ NPs, CS, and MoS$_2$-CS NPs were dispersed in deionized water under ultrasound assistance for the following characterizations. The hydrodynamic diameter was tested by dynamic light scattering using a Nano-ZS (Malvern Zeta sizer) system (Malvern, United Kingdom). The morphology, size, mapping and EDX were studied by TEM (H-750, HITACHI, Japan). Zeta potential measurements were performed using the Malvern ZS system. Fourier transform infrared (FT-IR) spectroscopy was performed using a Nicolet Avatar-330 spectrometer (Thermo Nicolet, United States). UV − vis absorption spectra were acquired using a Nicolet Evolution 300 UV − vis spectrometer (Thermo Nicolet, United States). Raman spectra was obtained using Raman spectroscopy (Renishaw, United Kingdom) equipped with a 785 nm laser. XRD of bulk MoS$_2$, MoS$_2$ NPs, CS and MoS$_2$-CS NPs powder was measured with Burker D8 (Burker, German).

### 2.4. Bacterial strain and growth conditions

The bacterial strains used in this study for evaluating the MoS$_2$-CS NPs activity of bacteria inhibition include *RM1021, Erwinia carotovora,* and *Xanthomonas citri*. *RM1021* was grown in Sager-Granick medium (SG) at 27 °C and 180 rpm for 24 h. *Erwinia carotovora* and *Xanthomonas citri* were grown in Nutrient Agar (NA) broth at 27 °C and 180 rpm for 24 h.

### 2.5. In vitro antibacterial activity of MoS$_2$ NPs and MoS$_2$-CS NPs

The antibacterial activities of MoS$_2$ NPs and MoS$_2$-CS NPs were evaluated using the dilution plate method and all experiments were repeated three times. *RM1021, Erwinia carotovora,* and *Xanthomonas citri* ($1.0 \times 10^6$ CFU/mL, 1 mL) cultured in SG and NA broth were incubated with different concentrations of MoS$_2$ NPs and MoS$_2$-CS NPs (0,15.625,31.25,62.5125, and 250 μg/mL) for 4 h at 27 °C, and the colonies of *RM1021, Erwinia carotovora,* and *Xanthomonas citri* were counted on SG and NA solid medium, respectively. The antibacterial activity of MoS$_2$ NPs and MoS$_2$-CS NPs was obtained with the following formula1 by the survival rate *RM1021, Erwinia carotovora,* and *Xanthomonas citri*.

$$\text{Survival rate (\%)} = \frac{[\text{Colonies (experimental group)}]}{[\text{Colonies (control group)}]} \times 100 \quad (1)$$

### 2.6. TEM analysis MoS$_2$-CS NPs effect on the cellular morphology of Xanthomonas citri

The effect of MoS$_2$-CS NPs on the cellular morphology of *Xanthomonas citri* was investigated by TEM. Then, $10^6$ CFU/mL of *Xanthomonas citri* suspended in the NA were treated with 250 μg/mL MoS$_2$-CS NPs for 2 h at 27 °C and 200 rpm. Subsequently, *Xanthomonas citri* collected at 3000 rpm for 5 min were fixed with 3 % glutaraldehyde for 1 h at room temperature. The fixed cells of *Xanthomonas citri* were centrifuged and dehydrated with a series of concentration ethanol gradients (10 %, 30 %, 50 %,70 %, 85 %,90 %, 95 % and 100 %). Dehydrated cells (20 μL) in 100 % ethanol were dropped on a copper mesh and observed under TEM. The treatment of control cells was paralleled with the MoS$_2$-CS NPs treatment.

### 2.7. In vivo CLas antibacterial activity of MoS$_2$-CS NPs

The 100 mg leaves samples collected were homogenized into powder after quick freezing in liquid nitrogen using a TissueLyser (JXFSTPRP-24, Jingxin, Shanghai, China). Then, total DNA was extracted using the DNeasy plant kit (Hlingene, Shanghai, China), following the manufacturer's instructions, and finally eluted in 50 μL nuclease-free water. The concentration was measured using a Nanodrop 2000c Spectrophotometer. The *C*Las inhibition activities of MoS$_2$-CS NPs were determined by qPCR with the primers for *C*Las (Table S1). The qPCR assays were carried out with Quantistudio3 using the 2× SYBR Green qPCR mix (Aidlab, Beijing, China) in a 10 μL reaction. The standard amplification protocol was 95 °C for 10 min followed by 40 cycles at 95 °C for 15 s, 60 °C for 20s, and 72 °C for 15 s. All reactions were conducted in triplicate with MoS$_2$-CS NPs treatment and water controls. The *C*Las inhibition rate of MoS$_2$-CS was described by the *C*Las survival rate and calculated using Eq. (2).

$$\text{Survival rate (\%)} = \frac{[\text{RQ (experimental group)}]}{[\text{RQ (control group)}]} \times 100 \quad (2)$$

### 2.8. TEM analysis of the MoS₂-CS NPs distribution

The TEM analysis was performed as previously described. Briefly, small sections of HLB-positive leaves and stems with non-treatment, injection of MoS₂-CS NPs, and spray of MoS₂-CS NPs were uniformly collected and transferred to 3 % glutaraldehyde overnight at 4 °C for fixation. Then, the leaf samples were placed in 2 % osmium tetroxide for post-fixation and then dehydrated by sequential treatment with 10, 20, 30, 40, 50, 60, 70, 80, 90, and 100 % (thrice) acetone for 10 min each time. The leaf samples were incubated sequentially in 50, 75, and 100 % (twice) Spurr's low-viscosity epoxy resin for 8 h each time, and the one-micrometer sections were cut with a glass knife by staining with methylene blue/azure A for 30 s and basic fuchsin (0.1 g in 10 mL of 50 % ethanol) for 30 s. The sections were observed under a Leitz Laborlux S compound microscope (Leica Microsystems, Wetzlar, Germany) to determine the appropriate location within the vascular system.

### 2.9. Plant enzyme activity and metabolites test

#### 2.9.1. Determination of chlorophylls and carotenoids content

The 100 mg leaf samples collected were homogenized into powder after quick freezing in liquid nitrogen using a TissueLyser from Jingxin (JXFSTPRP-24, Shanghai, China). The homogenized powder was diluted in 1 mL of ethanol and shaken at room temperature for 15 min. The supernatant was collected after centrifugation at 6000 rpm for 5 min. The powders of the tissues at the bottom of the 1.5 mL tube were washed with 1 mL ethanol, shaken at room temperature, and centrifuged at 6000 rpm for 5 min twice more. The absorbance of the supernatant was measured at 470, 649, and 665 nm, and the content and relative content of chlorophylls and carotenoids were calculated using Eqs. (3), (4), (5), (6), and (7), respectively.

$$C_a \, (\text{mg/L}) = 13.95A_{665} - 6.88A_{649} \tag{3}$$

$$C_b (\text{mg/L}) = 24.96A_{649} - 7.32A_{665} \tag{4}$$

$$C_{\text{total}} \, (\text{mg/L}) = C_a + C_b \tag{5}$$

$$C_{\text{carotenoid}} \, (\text{mg/L}) = (1000A_{470} - 3.27C_a - 104C_b)/229 \tag{6}$$

$$\text{Relative content (\%)} = \frac{[\text{Content (experimental groups)}]}{[\text{Content (control groups)}]} \times 100 \tag{7}$$

#### 2.9.2. Determination of MDA and soluble sugar

The 100 mg leaves samples collected were homogenized into powder after the quick freeze in liquid nitrogen using TissueLyser from Jingxin (JXFSTPRP-24, Shanghai, China). The homogenized powder was diluted in 1 mL of 10 % TCA and shaken at room temperature for 5 min. After centrifugation at 6000 rpm for 5 min, the supernatant (500 μL) was reacted with 500 μL 0.6 % TBA in a boiling water bath for 10 min. The mixed solution was placed on ice for rapid cooling and centrifuged at 3500 rpm for 10 min. The supernatant was measured at 450, 532, and 600 nm to determine the content and relative content of MDA and soluble sugar by following Eqs. (8), (9) and (7) respectively.

$$C_{\text{sugar}} \, (\mu\text{mol/L}) = 11.71A_{450} \tag{8}$$

$$C_{\text{MDA}} \, (\mu\text{mol/L}) = 6.45(A_{450} - A_{600}) - 0.56A_{450} \tag{9}$$

#### 2.9.3. Determination of starch

The 100 mg leaves samples collected were homogenized into powder after the quick freeze in liquid nitrogen using TissueLyser from Jingxin (JXFSTPRP-24, Shanghai, China). The homogenized powders were then diluted in 1 mL of 80 % calcium nitrate solution and heated at 95 °C for 5 min. After the solution turned colloidal, the supernatant was collected by centrifugation at 3000 rpm for 10 min. The starch colloidal solution 1 mL was mixed with 1 mL of 0.5 % iodine solution and stewed for 15 min.

After centrifugation at 3000 rpm for 5 min, the sediment was washed twice with an 80 % calcium nitrate solution containing 5 % iodine. The sediment was added to 1 mL of 0.1 mol/L NaOH and placed in boiling water for dissolution. The solution was then mixed with 300 μL 0.5 % iodine solution and 1 1 mL 0.1 mol/L HCL solution and measured at 590 nm. Starch content was calculated using a standard curve. Briefly, 0, 0.5, 1.0, 2.0, 3.0, 4.0, and 5.0 mL of 1.0 mg/mL starch solution were diluted into 5 mL with 80 % calcium nitrate solution and reacted with 2 mL of 5 % iodine for 15 min. The absorbance was measured at 590 nm after centrifugation at 3000 rpm for 5 min.

#### 2.9.4. Determination of H₂O₂

The 100 mg leaves samples collected were homogenized into powder after quick freezing in liquid nitrogen using a TissueLyser from Jingxin (JXFSTPRP-24, Shanghai, China). Then, the homogenized powders were diluted into approximately 900 μL 0.1 M PBS solution. $H_2O_2$ was extracted and quantified according to the manufacturer's instructions. The relative concentration of $H_2O_2$ was calculated using equantion7.

#### 2.9.5. Monitoring ROS of HLB-positive leaves

Three HLB-positive leaves treated with water and MoS₂-CS NPs were collected on the third day. After incubation with 5 μM DCFH (Cat. #D399, Thermo-Fisher Scientific), slices of veins and lamina were placed on microscope slides. DCFH fluorescence was visualized by confocal laser scanning microscopy (CLSM) (Leica TCS-SP5, Mannheim, Germany) with excitation/emission at 495 nm/525 nm.

#### 2.9.6. Determination of antioxidant enzyme activity

The 100 mg leaves samples collected were homogenized into powder after the quick freeze in liquid nitrogen using TissueLyser from Jingxin (JXFSTPRP-24, Shanghai, China). Then, the homogenized powders were diluted into around 900 μL 0.1 M PBS solution. CAT, POD, and SOD were extracted and calculated using responding assay kits from Nanjing Jiancheng Bioengineering Institute (Nanjing, China) according to the manufacturer's instructions. APX activity was detected by APX specifically catalysing $H_2O_2$ with the ASA thereby oxidised. Briefly, 3 mL reaction mixture of APX enzyme activity assay contained 50 mmol/L $K_2HPO_4$-$KH_2PO_4$ buffer (pH 7.0), 0.1 mmol/L EDTA-Na₂, 0.3 mmol/L AsA, 0.06 mmol/L $H_2O_2$ and 0.1 mL of APX enzyme solution. The change in absorbance at 290 nm was measured in 1 min at 20 °C and the 0.01 absorbance change at 290 nm per second was described as 1 U herein. The relative antioxidant enzyme activity was calculated using the equation10.

$$\text{Relative activity (\%)} = \frac{[\text{Enzyme activity (experimental group)}]}{[\text{Enzyme activity (control group)}]} \times 100 \tag{10}$$

### 2.10. Gene expression assays using reverse transcription quantitative PCR (RT-qPCR)

The 100 mg leaf samples collected were homogenized into powder after quick freezing in liquid nitrogen using a TissueLyser Jingxin (JXFSTPRP-24, Shanghai, China). Total RNA was extracted using the RNeasy Plant Mini Kit from Hlingene (Shanghai, China) according to the manufacturer's instructions. cDNA was synthesized using the NG Script I cDNA Synthesis Kit from Hlingene (Shanghai, China) according to the manufacturer's instructions and diluted 10 times for RT-qPCR. Reactions were carried out by mixing 1 μL cDNA, 1 μL each specific primer (Table S1), 2 μL deionized water, and 5 μL 2 × Sybr Green Master Mix from Hlingene (Shanghai, China) performed with QuantiStudio3 using the standard fast protocol of 95 °C for 10 min followed by 40 cycles at 95 °C for 15 s, 60 °C for 20s, and 72 °C for 15 s. Relative gene expression was calculated using the $2^{-\Delta\Delta CT}$ method. Except for the primers of *PAL*, *PR1*, and *PR2*, which have been previously reported [30], the rest of the primers were designed at NCBI.

### 2.11. Effect on soil microbial community

5 g of soil for HLB-positive sweet orange cultivation treated with 500 μL of 250 μg/mL MoS₂-CS NPs and water were collected in sterile tubes for analysis and stored in a refrigerator at −80 °C. The collected samples were sent in a blister box with dry ice to Azenta (www.genewiz.com.cn) to determine the effect of MoS₂-CS NPs on the soil microbial community using the Illumina MiSeq/NovaSeq platform with high-throughput sequencing of the V3–V4 region.

## 3. Results and discussion

### 3.1. Synthesis and characterization of MoS₂-CS NPs

A two-step approach was innovatively devised as an evolution of the one-step method for generating MoS₂-CS NPs [35], offering the ecological and simplified merits of the latter while rendering enhanced cost-effectiveness through the facile recycling of unexfoliated bulk MoS₂ within aqueous solutions. This two-step synthesis circumvented the utilization of harsh chemicals, such as lithium and oleum, which are conventionally employed in the synthesis of MoS₂ NPs. The process involves ultrasonic-mediated exfoliation of bulk MoS₂ into 2-D MoS₂ NPs and the combination of MoS₂ NPs and chitosan (Fig. 1a). Ultrasonication

disrupts the van der Waals interactions in layered MoS₂, resulting in the disintegration of bulk MoS₂ into individual nanoparticles through cavitation and bubble formation induced by high-frequency sonic waves in aqueous solutions [36]. Research indicates that ultrasonication of bulk MoS₂ generates sulfur vacancies and microcavities due to ultrasonic wave propagation, creating local hotspots with high temperature and pressure. These conditions facilitate the exfoliation process, resulting in the formation of few-layered MoS₂ NPs [37,38]. Subsequently, unexfoliated bulk MoS₂ was retrieved from the deposit, and dispersed MoS₂ NPs were introduced into a chitosan solution diluted with 0.2 % acetic acid. Under stirring, electrostatic interactions facilitated the formation of homogeneous MoS₂-CS NPs, comprising MoS₂ with a negative surface potential encapsulated by chitosan with an opposing surface potential. The resulting MoS₂-CS suspension was characterized and evaluated for its effectiveness against *Citrus* HLB.

Ultrasonic exfoliation significantly diminished the main particle size of bulk MoS₂ from 400 μm to 30 nm, confirming the acquisition of MoS₂ NPs. The subsequent increase in the main particle size of MoS₂-CS NPs from 30 nm to 70 nm was attributed to the CS surface modification of MoS₂ NPs (Fig. 1c), corroborated by the TEM images of bulk MoS₂, MoS₂ NPs, and MoS₂-CS NPs (Fig. 1b). Raman spectrum showed that the bulk MoS₂ exhibited peaks of $E_{2g}$ and $A_{1g}$ at 390 cm$^{-1}$ and 408 cm$^{-1}$, respectively, and the interval between $E_{2g}$ and $A_{1g}$ in the MoS₂ NPs and
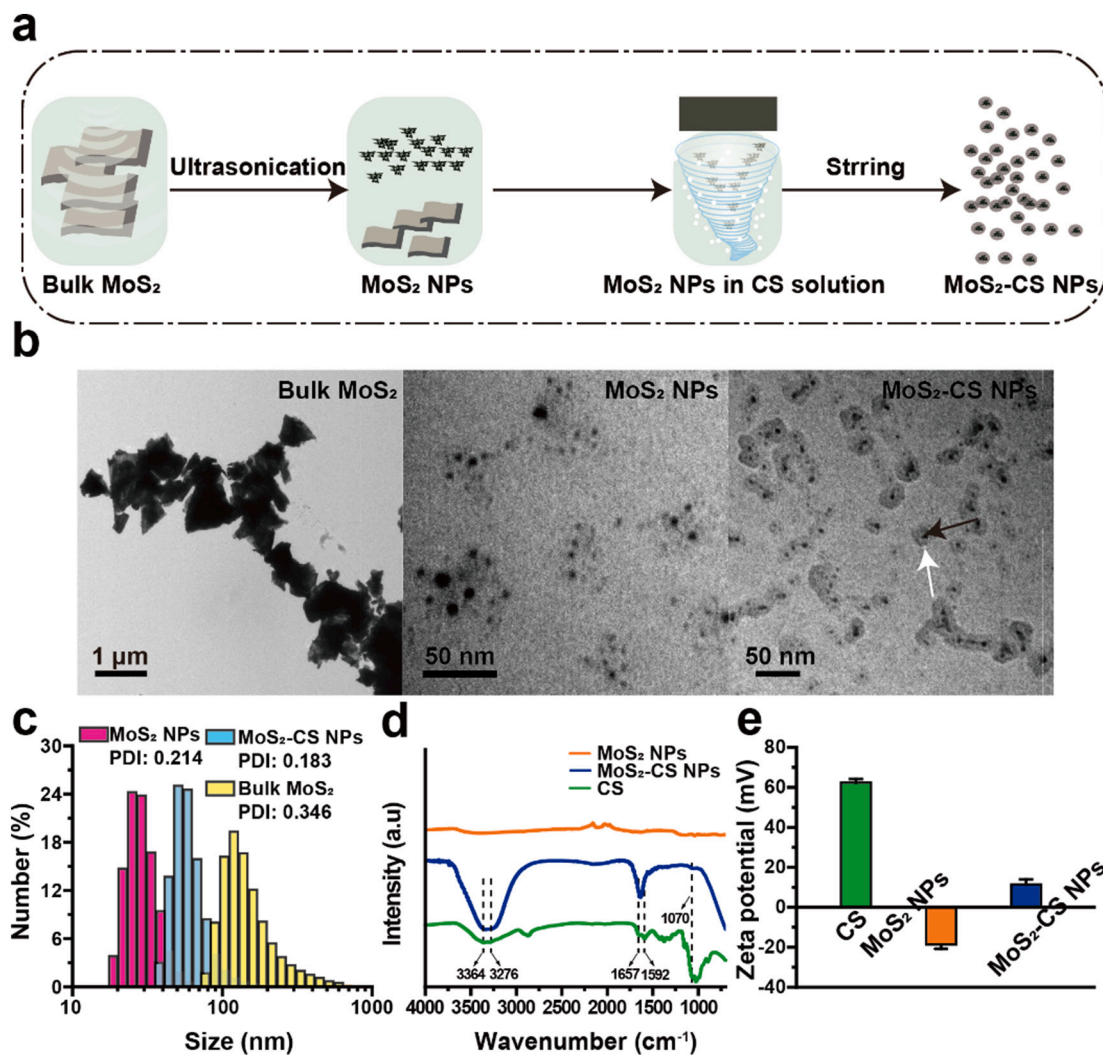


**Fig. 1.** Synthesis and characterization of MoS₂-CS NPs. Synthesis of MoS₂-CS by a two-step method (a). TEM images of Bulk MoS₂, MoS₂ NPs, and MoS₂-CS NPs (b). Hydrodynamic diameters of Bulk MoS₂, MoS₂ NPs, and MoS₂-CS NPs (c). FT-IR spectra of Bulk MoS₂, MoS₂-CS and CS (d). ζ potential of MoS₂ NPs, MoS₂-CS NPs, and CS (e).

MoS$_2$-CS NPs was shortened (Fig. S1a), which is evidence of the successful exfoliation of MoS$_2$ [39,40]. Evident similarities in FT-IR spectra between MoS$_2$-CS and CS, divergent from bulk MoS$_2$, showcased peaks at 1657 cm$^{-1}$ and 1592 cm$^{-1}$ corresponding to −C=O stretching of amide groups and − NH bending of secondary amide, respectively (Fig. 1d) [41]. Additionally, the spectra displayed sharp peaks at 1070 cm$^{-1}$, indicative of C-O bond stretching vibrations, observable in both MoS$_2$-CS and CS [42]. Moreover, characteristic peaks at 3276 cm$^{-1}$ and 3364 cm$^{-1}$ originating from N − H and O − H bond stretching vibrations were shared between CS and MoS$_2$-CS, absent in bulk MoS$_2$ [41,43]. The UV–vis absorption spectrum of MoS$_2$-CS NPs portrayed discernible adsorption peaks at 407, 450, 613, and 674 nm, aligning with single or few-layered 2H-MoS$_2$, affirming the successful ultrasonic exfoliation from bulk MoS$_2$ to MoS$_2$ NPs [44]. Peaks at 674 and 613 nm emanate from direct excitonic transitions at the K point of the Brillouin zone, whereas the 450 and 407 nm peaks correspond to direct excitonic transitions at the M point of the Brillouin zone. The absorbance profiles of MoS$_2$ NPs and CS solution showed similar peaks to that of MoS$_2$-CS NPs and no peak of maximum absorption (Fig. S1b).Compared with the multiple and sharp diffraction peaks of bulk MoS$_2$, MoS$_2$-CS NPs not only retained the signature peak which was also observed in MoS$_2$ NPs at ~14.2°, compatible with the 002 plane of 2-H MoS$_2$, but also exhibited the scattering peak of CS at ~19.8° (Fig. S1c and d), which could also successfully demonstrate the synthesis of MoS$_2$-CS NPs. The FT-IR spectra of bulk MoS$_2$, CS, and MoS$_2$-CS were compared (Fig. 1d). Surface charge evaluation revealed MoS$_2$-CS with a positive charge (+11.4 ± 2.6 mV), contrasting with the negative charge (−18.7 ± 2.1 mV) of bulk MoS$_2$, affirming the successful surface modification of CS with a positive charge (+62.4 ± 1.73 mV) onto MoS$_2$ NPs (Fig. 1e). The MoS$_2$ NPs after exfoliation and MoS$_2$-CS NPs were used for the in vitro antibacterial activity assay, as they showed more favorable dispersibility in aqueous solutions after 24 h compared to bulk MoS$_2$ and CS (Fig. S1h). Elemental mapping via TEM revealed a homogeneous distribution of chitosan, along with oxygen and nitrogen, predominantly in the periphery of the molybdenum and sulfur elements. This distribution is indicative of a core-shell architecture, with the chitosan-based components forming a shell around the core elements, that is consistent with the EDX linear scan (Fig. S1e–f, S2).

## 3.2. In vitro antibacterial activity of MoS$_2$-CS NPs

To ascertain the antibacterial potential of MoS$_2$-CS NPs against CLas, an in vitro antibacterial assessment was conducted after successful synthesis confirmation. Given the inability to culture CLas in vitro, three alternative gram-negative bacterial strains, Sinorhizobium meliloti RM1021, Erwinia carotovora, responsible for tomato soft rot, and Xanthomonas citri, the main pathogen of Citrus canker, were employed to gauge the in vitro antibacterial activity of MoS$_2$-CS NPs. The antibacterial activity of both MoS$_2$ NPs (Fig. S3a) and MoS$_2$-CS NPs (Fig. 2a) against RM1021 in the SG medium exhibited a conspicuous concentration-dependent antibacterial effect. As the concentration of MoS$_2$-CS NPs increased, the antibacterial activity proportionally intensified. Remarkably, at 250 μg/mL, the MoS$_2$-CS NP-treated group displayed a 7.40 % RM1021 survival rate, while the MoS$_2$ NP-treated group showed a 19.30 % ± 3.40 % survival rate. Across the remaining concentrations (15.625, 31.25, 62.5, and 125 μg/mL), MoS$_2$-CS NPs consistently outperformed MoS$_2$ NPs in terms of antibacterial efficacy, unequivocally corroborating the heightened antibacterial prowess attributed to the CS surface modification of MoS$_2$ NPs. The antibacterial effectiveness of MoS$_2$-CS and MoS$_2$ NPs against Erwinia carotovora and Xanthomonas citri showed a similar tendency to that of RM1021. The survival rate of the MoS$_2$-CS NP-treated group reached 8.94 % ± 1.40 % and 6.41 % ± 0.56 % at 250 μg/mL, respectively (Fig. 2b–c), while the MoS$_2$ NP-treated group only showed 28.67 % ± 0.96 % and 26.6 % ± 1.44 % at 250 μg/mL, respectively (Fig. S3b–c). This augmentation of antibacterial potency could be ascribed to the alteration of the MoS$_2$ nanoparticle surface potential from negative to positive, rendering them more amenable to interaction with gram-negative bacteria. The outcomes of the diluted plate assays for the in vitro antibacterial assessment were consistent with the survival rate (Fig. 2d and Fig. S3d). TEM was systematically conducted to scrutinise the cellular architecture of Xanthomonas citri in the control group, MoS$_2$ NPs, and MoS$_2$-CS NP-treated groups (Fig. S3e and 2e). The findings revealed the pristine rod-shaped cell structure of the control group, which was characterized by an intact cellular framework and smooth cell membrane. In contrast, the MoS$_2$ NP-treated group exhibited a remarkable ability to perforate Xanthomonas citri cells, and this puncture resulted in the release of cellular contents, ultimately leading to bacterial death. Within the MoS$_2$-CS
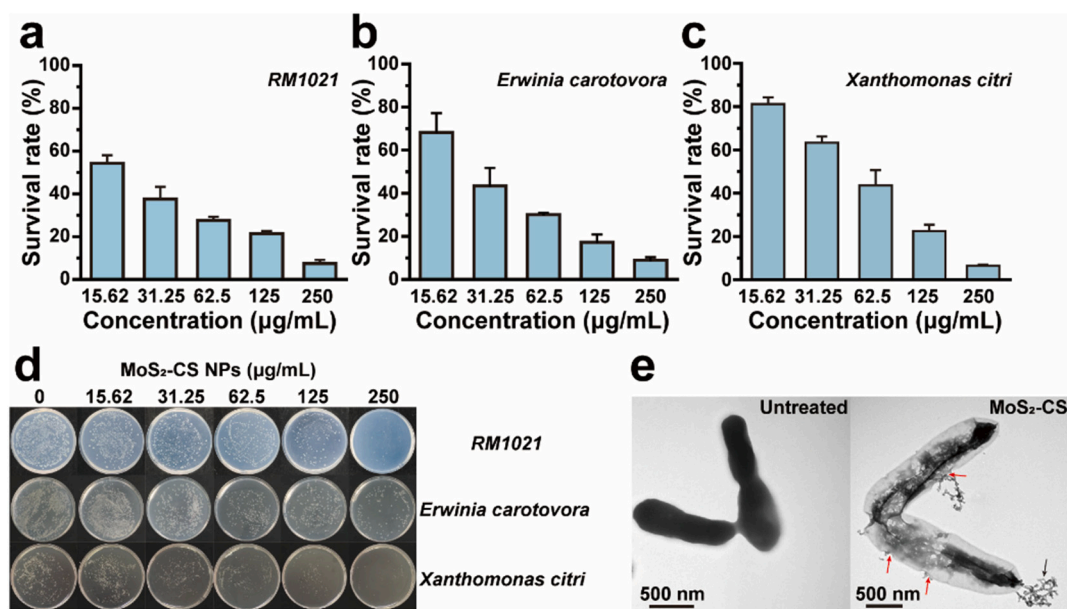


**Fig. 2.** In vitro antibacterial activity of MoS$_2$-CS NPs. The survival rate of RM1021 (a), Erwinia carotovora (b), and Xanthomonas citri (c) after treatment with different concentrations of MoS$_2$-CS NPs (15.62, 31.25, 62.5, 125, and 250 μg/mL). Dilution plates of SG and NA after treatment with different concentrations of MoS$_2$-CS NPs (15.625, 31.25, 62.5, 125, and 250 μg/mL) (d). TEM images of untreated and 250 μg/mL MoS$_2$-CS NP-treated Xanthomonas citri (e).

treatment group, a distinct interaction pattern emerged. The observations initially highlighted the MoS$_2$-CS NPs establishing surface contact with *Xanthomonas citri* cells. Notably, the bacterial cell membranes exhibited signs of crumpling in the vicinity of this contact, accompanied by the penetration of MoS$_2$-CS NPs into the bacterial cells, which led to the structural collapse of bacterial cells, culminating in the effective eradication of *Xanthomonas citri*. (See Fig. 2e).

### 3.3. Distribution of MoS$_2$-CS NPs in the phloem of HLB-positive leaves

To determine whether MoS$_2$-CS NPs could be distributed around *C*Las after foliar spraying, TEM analysis was conducted. Leaves treated with MoS$_2$-CS NPs on the third day were collected, using leaves injected with MoS$_2$-CS NPs and leaves sprayed with water as positive and negative controls, respectively. MoS$_2$-CS NPs were not observed in the leaves treated with water (Fig. 3a and d). Both the foliar spray and foliar injection routes of MoS$_2$-CS NPs exhibited their distribution within the phloem, with the numbers of *C*Las much lower than in those leaves treated solely with water, which contributed to the antibacterial activity of MoS$_2$-CS NPs. Notably, the foliar spray displayed a concentration akin to that of the foliar injection, rationalizing the consistent outcomes observed between the *in vitro* and *in vivo* antibacterial assays (Fig. 3c–e). Intriguingly, the size of the MoS$_2$-CS NPs observed in the phloem of HLB-positive leaves exceeded those observed *in vitro*. This phenomenon could be attributed to the attraction between gram-negative bacteria and MoS$_2$-CS NPs owing to their opposing surface potentials (Fig. 3c–f). Collectively, it was confirmed that MoS$_2$-CS NPs successfully permeated HLB-positive leaves and the phloem cells where *C*Las colonised, thereby enabling direct interaction with *C*Las.

### 3.4. In vivo antibacterial activity of MoS$_2$-CS NPs

Following the confirmation of significant *in vitro* antibacterial activity against *RM1021*, *Erwinia carotovora* and *Xanthomonas citri*, TEM graphs of *Xanthomonas citri* morphology after treatment with MoS$_2$-CS NPs and the distribution of MoS$_2$-CS NPs around *C*Las within the phloem, a plausible antibacterial mechanism for MoS$_2$-CS NPs against *C*Las is depicted (Fig. 4a). Upon the entry of MoS$_2$-CS NPs into the foliage of HLB-positive sweet orange, these nanoparticles effectively translocate within the phloem. Subsequent localization of the MoS$_2$-CS NPs occurred in close proximity to the *C*Las, leading to a consequential interaction with the pathogens. The interaction between MoS$_2$-CS NPs and *C*Las was marked by a notable disruption in the membranes of *C*Las, accompanied by leakage of cytoplasmic contents, and the inhibition of *C*Las proliferation, which is similar to the damage caused by MoS$_2$-CS NPs to *Xanthomonas citri* cells (Fig. 2e). To verify the antibacterial activity of MoS$_2$-CS NPs against *C*Las, an *in vivo* antibacterial assessment of MoS$_2$-CS NPs was performed in sweet oranges afflicted with HLB. Subsequently, 100 μL of 250 μg/mL MoS$_2$-CS NPs was topically applied to each HLB-positive leaf, and 100 μL of water served as the control treatment. Leaf samples were harvested on the first, third, fifth, seventh, and ninth days for quantifying *C*Las changes through quantitative polymerase chain reaction (qPCR), as outlined in the methods section. A notable decline in *C*Las numbers occurred within HLB-positive leaves subsequent to MoS$_2$-CS NPs treatment. Specifically, on the first, third, and fifth days post-treatment, *C*Las decreased by 30.62 % ± 1.48 %, 86.33 % ± 0.66 %, and 89.58 % ± 0.35 %, respectively, in comparison to that of the control group (Fig. 4b). Notably, the antibacterial efficacy on the fifth day was most consistent with the *in vitro* antibacterial assay outcomes, which was consistent with the concentration of foliar spray akin to the foliar injection (Fig. S3b and c). However, on the seventh and ninth days, *C*Las counts increased to 16.6 % ± 0.70 % and 25.61 % ± 1.4 %, respectively, demonstrating an ascending trend relative to the fifth day, although they remained lower than those in the control group (Fig. 4b). It is imperative to note that the mechanism behind the diminished *C*Las numbers, whether attributed to direct interaction or indirect effects, such as upregulated defense marker genes due to MoS$_2$-CS NPs, necessitates further exploration.
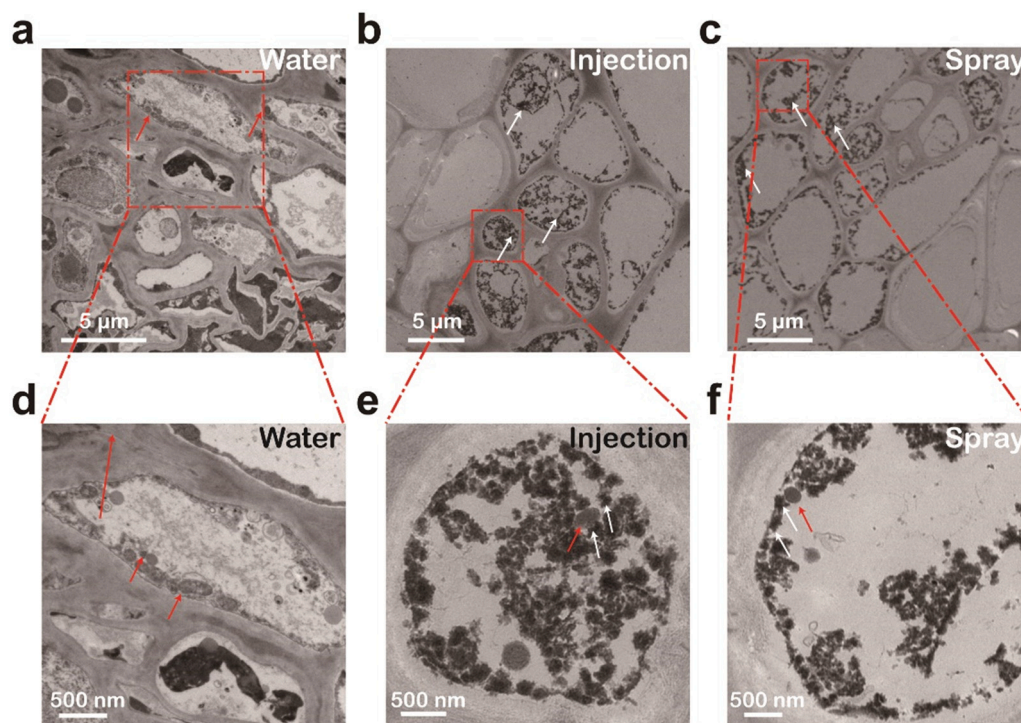


**Fig. 3.** TEM images of HLB-positive sweet orange leaves treated under various conditions. Leaves of HLB-positive sweet orange treated with (a) water, (b) injection of MoS$_2$-CS NPs, and (c) foliar spray of MoS$_2$-CS NPs. The enlarged sections of a (d), b (e), and c (f) show different distributions around *C*Las. The red dashed box, red arrow, and white arrow represent the enlarged section, *C*Las, and MoS$_2$-CS NPs, respectively. (For interpretation of the references to colour in this figure legend, the reader is referred to the web version of this article.)
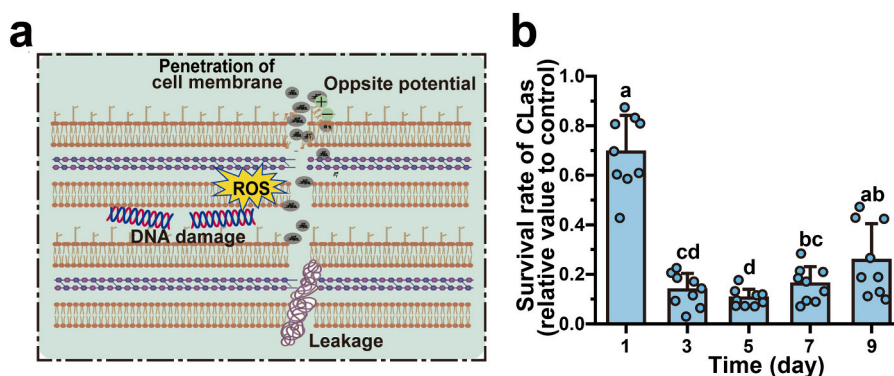
**Fig. 4.** *In vivo* antibacterial activity of MoS$_2$-CS NPs in the leaves of HLB-positive sweet orange. Schematic illustration of the antibacterial mechanism of MoS$_2$-CS NPs against *C*Las (a). The survival rate of *C*Las relative to the control group within 9 days after the treatment with MoS$_2$-CS NPs through qPCR (b).

### 3.5. Reduction of ROS by MoS$_2$-CS NPs

The conspicuous overproduction of H$_2$O$_2$ induced by *C*Las was deemed the prominent factor causing the symptoms in HLB-positive leaves [25]. In light of this, our investigation investigated the influence of MoS$_2$-CS NPs on H$_2$O$_2$ concentration in HLB-positive leaves. Specifically, the H$_2$O$_2$ concentration in HLB-positive leaves was diminished to 905.84 $\pm$ 49.54 µmol/g (Fig. 5a), situating it closer to the level observed in the healthy group rather than the untreated group. The variation in H$_2$O$_2$ concentration was collectively reduced within nine days after treatment with MoS$_2$-CS NPs (Fig. S4a).

ROS, which emerged during the redox reactions in plant, serves as one type of important signaling molecules involved in plant growth and resistance to stress [45]. However, excess reactive oxygen species may cause oxidative stress damage to plants leading to apoptosis [46]. ROS concentrate higher in HLB-positive sweet orange leaves than in healthy leaves which explains most HLB symptoms. Thus, the ROS in the vein and lamina of HLB-positive cells was detected using DCFH between the water and MoS$_2$-CS NPs treatment groups according to the lowest concentration of H$_2$O$_2$ on the third day after treatment with MoS$_2$-CS NPs. A drastic decrease in fluorescence in the MoS$_2$-CS NPs treatment compared to the water group both in the vein and lamina (Fig. 5b and Fig. S4b),

which implied the reduction of ROS level after treatment with MoS$_2$-CS NPs. Hence, we hypothesized that the antioxidant system in HLB-positive leaves was activated by treatment with MoS$_2$-CS NPs and explored the changes in four typical antioxidant enzymes (CAT, POD, SOD, and APX) in subsequent experiments.

### 3.6. Activation of HLB-positive leaves antioxidant system by MoS$_2$-CS NPs

Antioxidant enzymes, including CAT (catalase), POD (peroxidase), SOD (superoxide dismutase), and APX (ascorbate peroxidase), play an essential role in plants confronted with oxidative stress. These enzymes enable plants to counteract excessive peroxide anions, free radicals, hydrogen peroxide, and other ROS, which are principal culprits behind oxidative stress, thus ameliorating its impact [47,48]. Notably, the peak CAT and POD activity in HLB-positive leaves, reaching 212.60 $\pm$ 18.59 U/g and 223.17 $\pm$ 20.69 U/g respectively (Fig. 6a and Fig. S5a), manifested on the third day post MoS$_2$-CS NPs treatment. In contrast, the zenith of SOD and APX activity occurred on the fifth day after MoS$_2$-CS NPs treatment, culminating at 428.48 $\pm$ 32.36 U/g and 4.37 $\pm$ 0.39 U/g, respectively (Fig. 6b and Fig. S5b). The relative activity of CAT in HLB-positive leaves treated with MoS$_2$-CS NPs demonstrated substantial
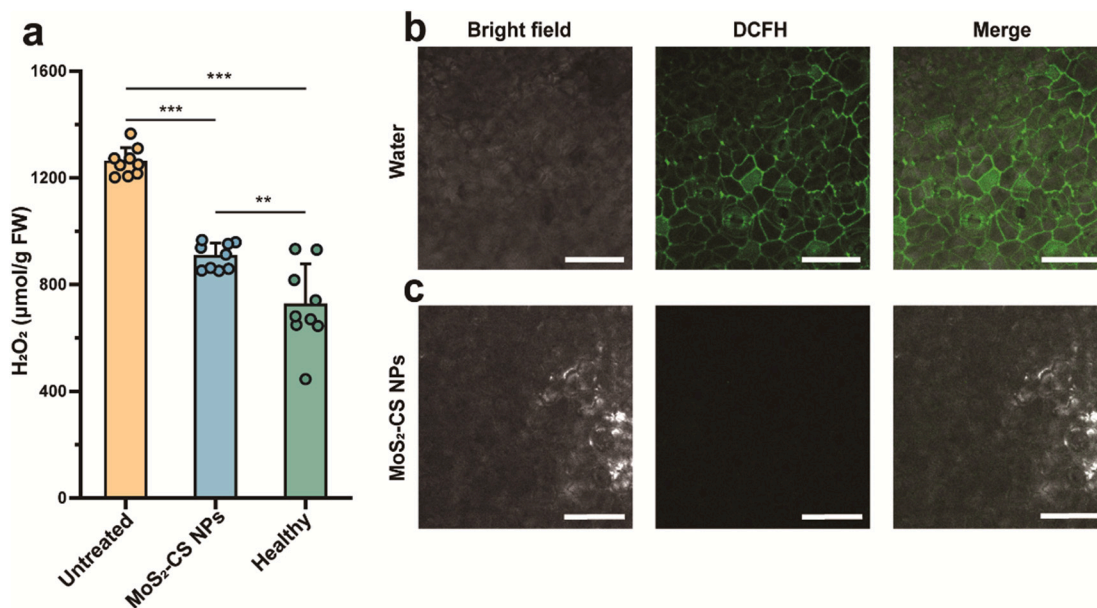


**Fig. 5.** Determination of ROS levels. The concentration of H$_2$O$_2$ (a). ROS levels in laminas treated with water (b) and MoS$_2$-CS NPs (c) were visualized using DCFH under a confocal laser microscope. Error bars represent SD ($n = 9$). ns, *, **, and *** indicate no significant difference, significant difference $P < 0.05$, $P < 0.01$, and $P < 0.001$, respectively.
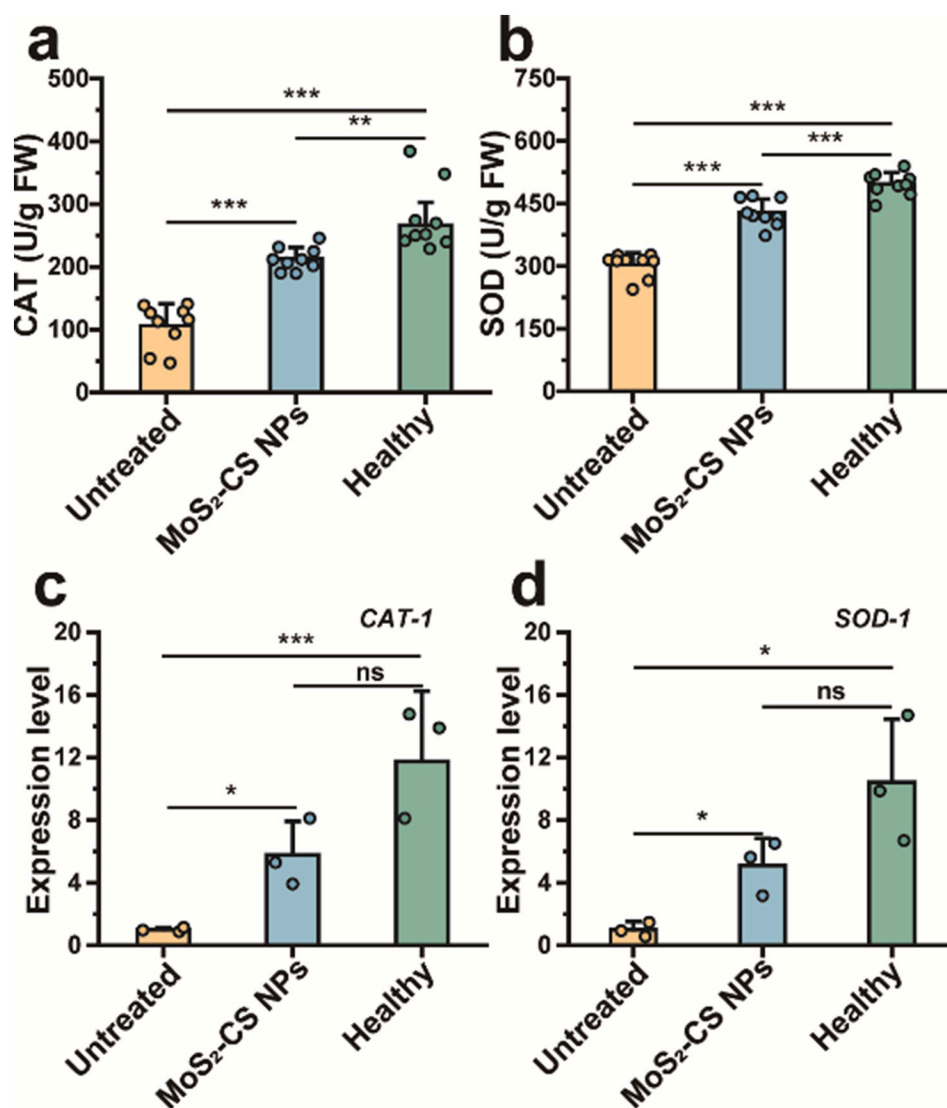
**Fig. 6.** Antioxidant enzyme activities and antioxidant-related gene expression levels in HLB-positive sweet orange leaves and healthy sweet orange leaves. Activities of CAT (a) and SOD (b). Error bars represent SD ($n = 9$). The expression level of *CAT-1* (c) and *SOD-1* (d). Error bars represent SD ($n = 3$). The ns, *, **, and *** stand for no significant difference, significant difference $P < 0.05$, $P < 0.01$, and $P < 0.001$, respectively.

enhancement, reaching 103.62 % ± 8.78 % relative to the control group on the ninth days near normal, respectively (Fig. S5c). Likewise, POD activity increased in HLB-positive leaves treated with MoS$_2$-CS NPs, reaching 111.30 % ± 5.57 %, 114.33 % ± 10.60 %, 113.50 % ± 3.50 %, 101.88 % ± 2.56 %, and 102.77 % ± 3.65 % relative to that of the control group on the respective days (Fig. S5d). Correspondingly, SOD activity increased in HLB-positive leaves treated with MoS$_2$-CS NPs, with values of 103.35 % ± 3.84 %, 112.83 % ± 2.85 %, 141.12 % ± 10.66 %, 120.52 % ± 4.36 %, and 108.03 % ± 8.41 % relative to that of the control group on the corresponding days (Fig. S5e). Similarly, APX activity showed an upsurge in HLB-positive leaves treated with MoS$_2$-CS NPs, registering values of 104.12 % ± 4.63 %, 122.80 % ± 4.62 %, 144.19 % ± 12.99 %, 117.24 % ± 7.18 %, and 109.82 % ± 15.26 % compared with that of the control group on the respective days (Fig. S5f). Despite HLB-positive leaves being subjected to excessive ROS attributed to *C*Las, the antioxidant enzyme levels in the HLB-positive group were notably lower than those in the WT group. This discrepancy suggests that HLB-positive leaves struggle to maintain ROS equilibrium through their intrinsic antioxidant systems, likely due to the down-regulation of antioxidant-related genes following *C*Las infestation [25]. The elevation in antioxidant enzyme activities may stem from

either MoS$_2$-CS NPs inducing the up-regulation of antioxidant-related genes in HLB-positive leaves *via* the provision of Mo elements, or the potential of MoS$_2$ NPs to function akin to antioxidant enzymes [24,49].

To reveal the potential mechanism of antioxidant enzyme activity enhancement, the relative expression levels of key antioxidant-related genes, including *CAT-1*, *CAT-2*, *SOD-1*, *SOD-2*, *POD*, *APX*, and *RbohA* (serving as crucial markers to validate the mitigation of oxidative stress), were scrutinized through precise RT-qPCR analysis. Additionally, defense marker genes, namely *PR-1*, *PR-2*, and *PAL*, were assessed.

Upon treatment with MoS$_2$-CS NPs, the upregulation of *CAT-1* and *SOD-1* genes became apparent within HLB-positive leaves, amplifying their expression by 5.78 ± 1.94-fold and 4.53 ± 1.87-fold, respectively (Fig. 6c and d). The variations in *CAT-1*, *CAT-2*, *SOD-1*, *SOD-2*, *APX*, and *POD* relative expression levels of HLB-positive sweet orange leaves within nine days after MoS$_2$-CS NPs treatment are shown in the SI (Fig. S6b–e), which were consistent with the fluctuation of corresponding antioxidant enzymes. The oscillation of *RbohA*, reflective of heightened oxidative stress within HLB-positive leaves, demonstrated a diametrically opposite trajectory to the aforementioned genes, plummeting to a nadir of 10.39 % ± 0.01 % relative to the control group following MoS$_2$-CS NPs treatment (Fig. S6f). In summary, the

application of MoS₂-CS NPs on HLB-positive leaves mitigated oxidative stress compared to the control group, indicating that alterations in antioxidant enzyme activities were, to some extent, attributed to the ebb and flow of antioxidant-related gene expression.

The induction of defense marker genes, *PR-1* and *PR-2*, both responsive to SA (salicylic acid) and integral to SAR (systemic acquired resistance), emerged as a salient outcome of MoS₂-CS NPs treatment. On the third day post-treatment, these genes were remarkably upregulated by 4.55 ± 0.68-fold and 3.40 ± 0.86-fold, respectively, relative to the control group (Fig. S6i–j). Additionally, PAL, a linchpin in the synthesis of phenylalanine ammonia-lyase (PAL) pivotal for plant defense against pathogenic bacteria, surged conspicuously on the third day, reaching a 4.41 ± 0.34-fold increase relative to the control group (Fig. S6k). This elevation is consistent with the expression trends of *PR-1* and *PR-2*. The up regulatory impact of MoS₂-CS NPs on these genes is conceivably linked to the contributory influence of CS, as previously postulated [50].

### 3.7. Improvement of physiological indices by MoS₂-CS NPs

To assess the comprehensive effect of MoS₂-CS NPs on HLB-positive sweet orange, physiological indices including MDA, soluble sugar, starch, and total chlorophyll content were evaluated. The level of MDA, a marker of lipid peroxidation in plant cell membranes, and soluble sugars, indicators of adverse conditions like drought, salt stress, and low temperature encountered by plants, [51,52] it was decreased to 8.33 ± 1.06 nmol/g and 106.70 ± 15.46 μmol/g on the third day post MoS₂-CS NPs treatment, which was significantly lower than the control group (Fig. 7a and b). In HLB-positive leaves of sweet orange, the MDA and soluble sugar content are much higher than those in healthy leaves, [53] indicating the severe adversity stress caused by CLas-induced oxidative stress. The relative changes in MDA and soluble sugar levels are shown in the SI (Fig. S7a and b). This observation underscores that MoS₂-CS

NPs did not induce biotic stress in HLB-positive leaves. Moreover, these nanoparticles appeared to mitigate the adverse stresses experienced by HLB-positive leaves. It is postulated that the excessive accumulation of ROS induced by CLas, reaching a critical threshold, potentially triggers the death of companion and sieve element cells. This oxidative stress is believed to contribute to higher MDA concentrations in HLB-positive leaves compared to healthy leaves [25,54].

Starch accumulation, one of the most prominent symptoms within HLB-positive sweet orange leaves, was also detected. The starch content reached 17.08 ± 4.01 mg/g, a lowest level which was significantly lower than that of control group (Fig. 7c), on the fifth day after MoS₂-CS NPs treatment (Fig. S7c).

CLas-induced excess ROS is recognized as a positive regulator of callose deposition, a phenomenon deleterious to chloroplast structure, leading to chlorophyll content reduction [25,55]. To better understand the effect of MoS₂-CS NPs treatment, the relative levels of chlorophyll and carotenoid were investigated (Fig. S7d–g). MoS₂-CS NPs (260.0244 ± 26.98 mg/g) treatment significantly increased total chlorophyll compared to the control group (Fig. 7d). Notably, HLB-positive leaves subjected to water treatment exhibited a distinct and progressive manifestation of yellowing symptoms. In contrast, the leaves treated with MoS₂-CS NPs displayed a starkly contrasting pattern, with a pause in conspicuous and progressive yellowing symptoms.

In summary, the reduction in MDA and soluble sugars underscored that MoS₂-CS NPs did not induce biotic stress in HLB-positive leaves. Moreover, these nanoparticles appeared to mitigate the adverse stresses experienced by HLB-positive leaves. Additionally, the mitigation of starch content also represented the effect of MoS₂-CS NPs treatment on HLB-positive leaves. The enhancement effect of MoS₂-CS NPs on chlorophyll content relative to control group aligns with the elevation of nitrogen source assimilation facilitated by MoS₂ [56,57]. Elevated chlorophyll content facilitates heightened light absorption, thereby
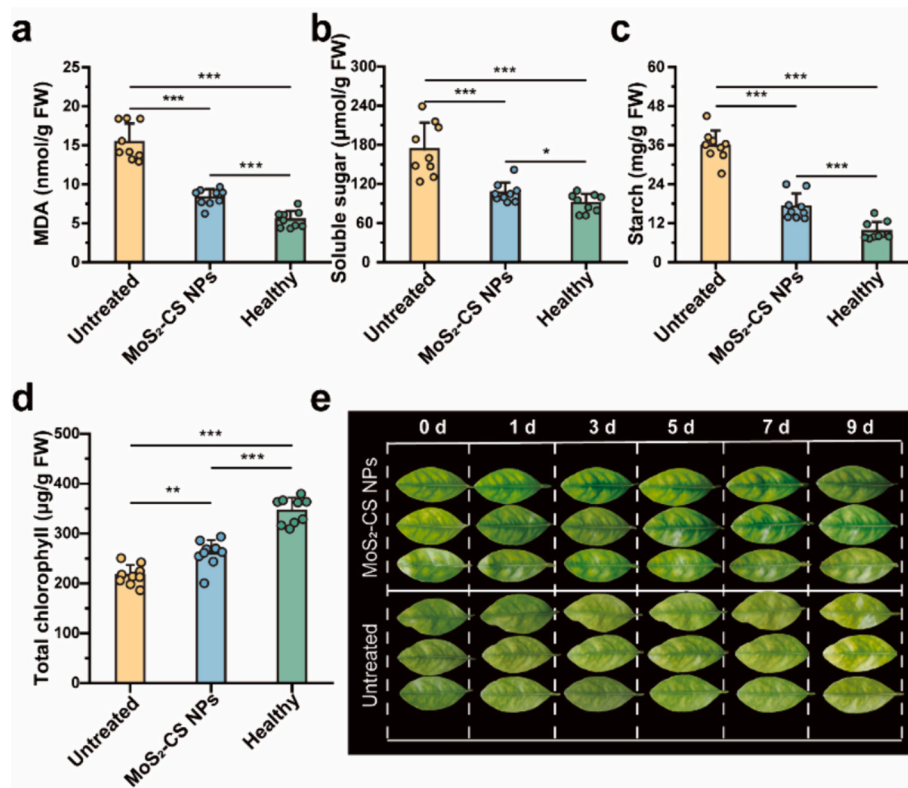


**Fig. 7.** Physiological indices of HLB-positive and healthy sweet orange leaves. MDA content (a), soluble sugars (b), starch (c), and total chlorophyll (d). Error bars represent SD ($n = 9$). ns, *, **, and *** indicate no significant difference, significant difference $P < 0.05$, $P < 0.01$, and $P < 0.001$, respectively. Photographs of the HLB-positive sweet orange leaves after non-treatment (untreated) and treatment with MoS₂-CS NPs within 9 days (e).

bolstering photosynthetic potential, and resulting in increased photosynthetic product generation [58], simultaneously showing the pause of progressive manifestation of yellowing symptoms. To conclude, MoS$_2$-CS NPs treatment is not toxic to HLB-positive leaves; rather, it effectively improved the physiological indices within HLB-positive leaves.

### 3.8. Biosafety of MoS$_2$-CS NPs in the soil

MoS$_2$ NPs could cause the negative impact on soybean- rhizobia symbiotic system through weakening the activity of rhizobium [59]. Although MoS$_2$-CS NPs were used to treat HLB-positive sweet orange by foliar spraying, the potential toxicity to the soil microbiome still needs to be considered. To investigate whether MoS$_2$-CS NPs exhibit toxicity to bacteria in the soil, analysis of soil bacterial diversity was conducted.

The species distribution of the soil microbial community showed the same trend between the untreated soil samples and MoS$_2$-CS NPs-treated samples (Fig. 8a). The indices for the evaluation of species diversity and complexity of samples showed a slight elevation in MoS$_2$-CS NPs-treated samples compared to untreated samples (Fig. 8b). The heat map shows the 30 most abundant genus after non-treatment and MoS$_2$-CS NPs

treatment, in which the blue blocks represent higher abundances relative to the control samples (Fig. 8c). After the analysis of the most different strains in the soil treated with MoS$_2$-CS NPs, a significant elevation in the relative abundance of the bacterial genera *Halomonas*, *Marinobacter*, *Limnobacter*, and *Sphingomonas* was noted in treated soils (Fig. 8d). These genera are instrumental in the mineralization of organic matter, thereby releasing nutrients such as carbon, nitrogen, phosphorus, and sulfur, which are vital for plant nutrition. The conversion of organic to inorganic forms of nutrients by these bacteria is a critical component of nutrient cycling within the soil. Furthermore, their decomposition activities contribute to soil aggregation, enhancing soil structural integrity and physical properties, including aeration and water-holding capacity. The observed enrichment of these decomposer bacteria underscores their fundamental role in maintaining the resilience and stability of the soil microbial communities. Collectively, Microbiome analysis elucidated to some extent an overall microbial abundance between soil samples treated with MoS$_2$-CS NPs and untreated controls, verifying the biosafety of MoS$_2$-CS NPs in the soil. Moreover, the result of four relatively abundant bacteria indicated the benefits of MoS$_2$-CS NPs to the soil microenvironment.
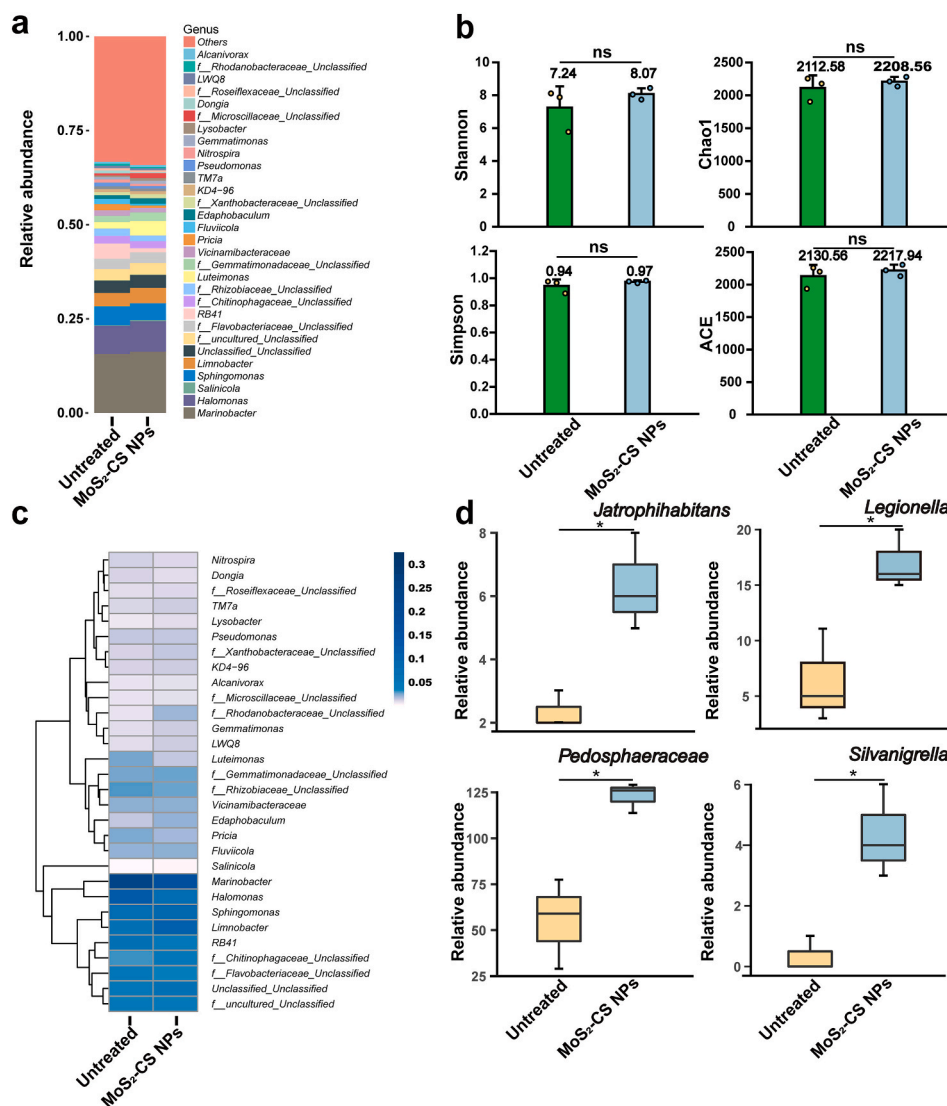


**Fig. 8.** Effect of MoS$_2$-CS NPs on the soil microbiome. Species distribution in the soil microbial community (a). Shannon, Chao 1, Simpson, and ACE indices for the soil microbial community with nontreatment and MoS$_2$-CS NPs treatment (b). Heat map analysis of the 30 most abundant genus after non-treatment and MoS$_2$-CS NPs treatment (c). Differences in strains after MoS$_2$-CS NPs treatment in the soil (d). Error bars represent SD ($n = 3$). The ns, *, **, and *** stand for no significant difference, significant difference $P < 0.05$, $P < 0.01$, and $P < 0.001$, respectively.

## 4. Conclusion

In conclusion, this study presents a novel approach for the synthesis of MoS$_2$-CS NPs, which exhibits dual advantages: augmenting chlorophyll content and bolstering plant antioxidant systems, alongside exceptional antibacterial efficacy against *C*Las. In particular, this antibacterial potency is achieved without reliance on photo-thermal stimulation, owing to surface modification with biocompatible chitosan. Consequently, a comprehensive strategy for addressing *Citrus* Huanglongbing has emerged, encompassing both the inhibition of *C*Las and the mitigation of *C*Las-induced adversities. This study introduces a new dimension to *Citrus* Huanglongbing treatment, underscoring the potential for multifaceted solutions facilitated by the design of nanomaterials with composite functionalities. Moreover, it extends the application of MoS$_2$ to agricultural antimicrobial domains, further augmenting its utility.

## CRediT authorship contribution statement

**Guiyun Deng:** Writing – review & editing, Writing – original draft, Visualization, Validation, Supervision, Software, Resources, Project administration, Methodology, Investigation, Funding acquisition, Formal analysis, Data curation, Conceptualization. **Feifan Lu:** Writing – review & editing, Writing – original draft, Visualization, Validation, Supervision, Software, Resources, Project administration, Methodology, Investigation, Funding acquisition, Formal analysis, Data curation, Conceptualization. **Shuojun Li:** Visualization, Validation, Supervision, Software, Resources, Project administration, Methodology, Investigation, Funding acquisition, Formal analysis, Data curation, Conceptualization. **Yuying Long:** Supervision, Software. **Jianghong Wu:** Resources. **Xiaofeng Guo:** Data curation. **Chunyin Li:** Visualization. **Zhiyong Song:** Visualization, Validation, Supervision, Software, Resources, Project administration. **Mohamed F. Foda:** Writing – review & editing. **Fang Ding:** Writing – review & editing, Writing – original draft, Visualization, Validation, Supervision, Funding acquisition. **Heyou Han:** Writing – review & editing, Writing – original draft, Visualization, Validation, Supervision, Software, Resources, Project administration, Methodology, Investigation, Funding acquisition, Formal analysis, Data curation, Conceptualization.

## Declaration of competing interest

The authors declare that they have no known competing financial interests or personal relationships that could have appeared to influence the work reported in this paper.

## Acknowledgment

## Appendix A. Supplementary data

Supplementary data to this article can be found online at https://doi.org/10.1016/j.ijbiomac.2024.135528.

## References

[1] A. Singerman, M.E. Rogers, The economic challenges of dealing with *Citrus* greening: the case of Florida, J. Integr. Pest Manag. 11 (1) (2020) 1.

[2] C. Su, F. Ding, W.J. Wang, Z.Y. Song, Q. Ali, M. Ali, N. Hong, G.P. Wang, H.Y. Han, Time-resolved fluorescent microsphere lateral flow biosensors for rapid detection of *Candidatus* Liberibacter asiaticus, Plant Biotechnol. J. 20 (7) (2022) 1235.

[3] J. Graham, T. Gottwald, M. Setamou, Status of Huanglongbing (HLB) outbreaks in Florida, California and Texas, Trop. Plant Pathol. 45 (3) (2020) 265.

[4] M.L. Bao, Z. Zheng, J.C. Chen, X.L. Deng, Investigation of *Citrus* HLB symptom variations associated with "*Candidatus* Liberibacter asiaticus" strains harboring different phages in southern China, Agronomy-Basel 11 (11) (2021) 2262.

[5] X. Chen, Y. Song, C. Ling, Y. Shen, X. Zhan, B. Xing, Fate of emerging antibiotics in soil-plant systems: a case on fluoroquinolones, Sci. Total Environ. 951 (2024) 175487.

[6] F.M. Aarestrup, N. Frimodt-Møller, Increasing transmission of antibiotic resistance from animals to humans, Ugeskr. Laeger 173 (36) (2011) 2180.

[7] R.R. Naik, A.A. Roy, S. Mutalik, N. Dhas, Unleashing the power of polymeric nanoparticles - creative triumph against antibiotic resistance: a review, Int. J. Biol. Macromol. 278 (2024) 134977.

[8] Y.T. Liu, K. Li, B. Liu, S.S. Feng, A strategy for precision engineering of nanoparticles of biodegradable copolymers for quantitative control of targeted drug delivery, Biomaterials 31 (35) (2010) 9145.

[9] M.J. Mitchell, M.M. Billingsley, R.M. Haley, M.E. Wechsler, N.A. Peppas, R. Langer, Engineering precision nanoparticles for drug delivery, Nat. Rev. Drug Discov. 20 (2) (2021) 101.

[10] N. Baig, I. Kammakakam, W. Falath, Nanomaterials: a review of synthesis methods, properties, recent progress, and challenges, Mater. Adv. 2 (6) (2021) 1821.

[11] W.S. Blaner, I.O. Shmarakov, M.G. Traber, Vitamin a and vitamin E: will the real antioxidant please stand up, Annu. Rev. Nutr. 41 (2021) 105.

[12] X. Lu, X. Gu, Y. Shi, A review on lignin antioxidants: their sources, isolations, antioxidant activities and various applications, Int. J. Biol. Macromol. 210 (2022) 716.

[13] B. An, Y. Wang, Y. Huang, X. Wang, Y. Liu, D. Xun, G.M. Church, Z. Dai, X. Yi, T. C. Tang, C. Zhong, Engineered living materials for sustainability, Chem. Rev. 123 (5) (2023) 2349.

[14] X. Li, H. Wang, J. Li, Z. Mao, S. Zhang, S. Zhao, M. Li, X. Hao, F. Peng, Plant cell wall inspired lignin-based membrane with configurable radical scavenging activity, Chem. Eng. J. 495 (2024) 153317.

[15] X. Hao, Z. Lv, H. Wang, J. Rao, Q. Liu, B. Lü, F. Peng, Top-down production of sustainable and scalable hemicellulose nanocrystals, Biomacromolecules 23 (11) (2022) 4607.

[16] V. Agarwal, K. Chatterjee, Recent advances in the field of transition metal dichalcogenides for biomedical applications, Nanoscale 10 (35) (2018) 16365.

[17] C. Liu, D.S. Kong, P.C. Hsu, H.T. Yuan, H.W. Lee, Y.Y. Liu, H.T. Wang, S. Wang, K. Yan, D.C. Lin, P.A. Maraccini, K.M. Parker, A.B. Boehm, Y. Cui, Rapid water disinfection using vertically aligned MoS$_2$ nanofilms and visible light, Nat. Nanotechnol. 11 (12) (2016) 1098.

[18] V. Yadav, S. Roy, P. Singh, Z. Khan, A. Jaiswal, 2D MoS$_2$-based nanomaterials for therapeutic, bioimaging, and biosensing applications, Small 15 (1) (2019) 1803706.

[19] J.K. Carrow, K.A. Singh, M.K. Jaiswal, A. Ramirez, G. Lokhande, A.T. Yeh, T. R. Sarkar, I. Singh, A.K. Gaharwar, Photothermal modulation of human stem cells using 2D nanomaterials, Proc. Natl. Acad. Sci. 117 (24) (2020) 13329.

[20] S. Pandit, S. Karunakaran, S.K. Boda, B. Basu, M. De, High antibacterial activity of functionalized chemically exfoliated MoS$_2$, ACS Appl. Mater. Interfaces 8 (46) (2016) 31567.

[21] J.J. Fan, Y.F. Li, H.N. Nguyen, Y. Yao, D.F. Rodrigues, Toxicity of exfoliated-MoS$_2$ and annealed exfoliated-MoS$_2$ towards planktonic cells, biofilms, and mammalian cells in the presence of electron donor, Environ. Sci.: Nano 2 (4) (2015) 370.

[22] A. Kumar, N.C. Aery, Biochemical changes, biomass production, and productivity of *Triticum aestivum* as a function of increasing molybdenum application, J. Plant Nutr. 46 (10) (2023) 2351.

[23] L.J. Zhao, S. Chen, X.J. Tan, X. Yan, W.H. Zhang, Y.X. Huang, R. Ji, A.O. White, Environmental implications of MoS$_2$ nanosheets on rice and associated soil microbial communities, Chemosphere 291 (2022) 133004.

[24] T.M. Chen, H. Zou, X.J. Wu, C.C. Liu, B. Situ, L. Zheng, G.W. Yang, Nanozymatic antioxidant system based on MoS$_2$ nanosheets, ACS Appl. Mater. Interfaces 10 (15) (2018) 12453.

[25] W.X. Ma, Z.Q. Pang, X.E. Huang, J. Xu, S.S. Pandey, J.Y. Li, D.S. Achor, F.N. C. Vasconcelos, C. Hendrich, Y.X. Huang, W.T. Wang, D. Lee, D. Stanton, N. Wang, *Citrus* Huanglongbing is a pathogen-triggered immune disease that can be mitigated with antioxidants and gibberellin, Nat. Commun. 13 (1) (2022) 529.

[26] S. Kwakye, D.M. Kadyampakeni, Micronutrients improve growth and development of HLB-affected *Citrus* trees in Florida, Plants-Basel 12 (1) (2023) 73.

[27] O. Pérez-González, R. Gomez-Flores, P. Tamez-Guerra, Insight into biological control potential of against Asian *Citrus* psyllid as a vector of *Citrus* Huanglongbing disease in America, J. Fungi 8 (6) (2022) 573.

[28] Q. Gao, X. Zhang, W.Y. Yin, D.Q. Ma, C.J. Xie, L.R. Zheng, X.H. Dong, L.Q. Mei, J. Yu, C.Z. Wang, Z.J. Gu, Y.L. Zhao, Functionalized MoS$_2$ nanovehicle with near-infrared laser-mediated nitric oxide release and photothermal activities for advanced bacteria-infected wound therapy, Small 14 (45) (2018) 1802290.

[29] W.T. Zhang, S. Shi, Y.R. Wang, S.X. Yu, W.X. Zhu, X. Zhang, D.H. Zhang, B. W. Yang, X. Wang, J.L. Wang, Versatile molybdenum disulfide based antibacterial composites for *in vitro* enhanced sterilization and *in vivo* focal infection therapy, Nanoscale 8 (22) (2016) 11642–11648.

[30] C.Y. Huang, K. Araujo, J.N. Sanchez, G. Kund, J. Trumble, C. Roper, K.E. Godfrey, H.L. Jin, A stable antimicrobial peptide with dual functions of treating and preventing *Citrus* Huanglongbing, Proc. Natl. Acad. Sci. U. S. A. 118 (6) (2021) 2019628118.

[31] M. Pitino, K. Sturgeon, C. Dorado, L.M. Cano, J.A. Manthey, R.G. Shatters, L. Rossi, Quercus leaf extracts display curative effects against *Candidatus* Liberibacter asiaticus that restore leaf physiological parameters in HLB-affected *Citrus* trees, Plant Physiol. Biochem. 148 (2020) 70.

[32] J.L.S.H. Stephano-Hornedo, O.T.G. Torres-Gutierrez, Y.T.M. Toledano-Magana, I. G.M. Gradilla-Martinez, A.P. Pestryakov, A.S.G. Sanchez-Gonzalez, J.C.G. R. Garcia-Ramos, N.B. Bogdanchikova, Argovit (TM) silver nanoparticles to fight Huanglongbing disease in Mexican limes (*Citrus aurantifolia* Swingle), RSC Adv. 10 (11) (2020) 6146.

[33] M. Chandrasekaran, M. Paramasivan, Chitosan derivatives act as a bio-stimulants in plants: a review, Int. J. Biol. Macromol. 271 (Pt 1) (2024) 132720.

[34] K.A. Abu-Sbeih, G.M. Al-Mazaideh, W.A. Al-Zereini, Production of medium-sized chitosan oligomers using molecular sieves and their antibacterial activity, Carbohydr. Polym. 295 (2022) 119889.

[35] S. Roy, A. Mondal, V. Yadav, A. Sarkar, R. Banerjee, P. Sanpui, A. Jaiswal, Mechanistic insight into the antibacterial activity of chitosan exfoliated $MoS_2$ nanosheets: membrane damage, metabolic inactivation, and oxidative stress, ACS Appl. Bio Mater. 2 (7) (2019) 2738.

[36] W. Qiao, S.M. Yan, X.M. He, X.Y. Song, Z.W. Li, X. Zhang, W. Zhong, Y.W. Du, Effects of ultrasonic cavitation intensity on the efficient liquid-exfoliation of $MoS_2$ nanosheets, RSC Adv. 4 (92) (2014) 50981.

[37] H. Xu, B.W. Zeiger, K.S. Suslick, Sonochemical synthesis of nanomaterials, Chem. Soc. Rev. 42 (7) (2013) 2555.

[38] S.V. Selvi, A. Prasannan, S.M. Chen, A. Vadivelmurugan, H.C. Tsai, J.Y. Lai, Glutathione and cystamine functionalized MoS(2)core-shell nanoparticles for enhanced electrochemical detection of doxorubicin, Mikrochim. Acta 188 (2) (2021) 35.

[39] E.P. Nguyen, B.J. Carey, T. Daeneke, J.Z. Ou, K. Latham, S. Zhuiykov, K. Kalantar-zadeh, Investigation of two-solvent grinding-assisted liquid phase exfoliation of layered MoS, Chem. Mater. 27 (1) (2015) 53.

[40] H. Li, J. Wu, Z. Yin, H. Zhang, Preparation and applications of mechanically exfoliated single-layer and multilayer $MoS_2$ and $WSe_2$ nanosheets, Acc. Chem. Res. 47 (4) (2014) 1067.

[41] D. Wang, L. Song, K.Q. Zhou, X.J. Yu, Y. Hu, J. Wang, Anomalous nano-barrier effects of ultrathin molybdenum disulfide nanosheets for improving the flame retardance of polymer nanocomposites, J. Mater. Chem. A 3 (27) (2015) 14307.

[42] X.M. Feng, X. Wang, W.Y. Xing, K.Q. Zhou, L. Song, Y. Hu, Liquid-exfoliated $MoS_2$ by chitosan and enhanced mechanical and thermal properties of chitosan/$MoS_2$ composites, Compos. Sci. Technol. 93 (2014) 76.

[43] W.Y. Yin, L. Yan, J. Yu, G. Tian, L.J. Zhou, X.P. Zheng, X. Zhang, Y. Yong, J. Li, Z. J. Gu, Y.L. Zhao, High-throughput synthesis of single-layer $MoS_2$ Nanosheets as a near-infrared Photothermal-triggered drug delivery for effective cancer therapy, ACS Nano 8 (7) (2014) 6922.

[44] W.T. Zhang, Y.R. Wang, D.H. Zhang, S.X. Yu, W.X. Zhu, J. Wang, F.Q. Zheng, S. X. Wang, J.L. Wang, A one-step approach to the large-scale synthesis of functionalized $MoS_2$ nanosheets by ionic liquid assisted grinding, Nanoscale 7 (22) (2015) 10210.

[45] J.S. Qi, J.L. Wang, Z.Z. Gong, J.M. Zhou, Apoplastic ROS signaling in plant immunity, Curr. Opin. Plant Biol. 38 (2017) 92.

[46] J.L. Montillet, S. Chamnongpol, C. Rustérucci, J. Dat, B. van de Cotte, J.P. Agnel, C. Battesti, D. Inzé, F. Van Breusegem, C. Triantaphylidès, Fatty acid hydroperoxides and $H_2O_2$ in the execution of hypersensitive cell death in tobacco leaves, Plant Physiol. 138 (3) (2005) 1516.

[47] K. Asada, Ascorbate peroxidase - a hydrogen peroxide-scavenging enzyme in plants, Physiol. Plant. 85 (2) (1992) 235.

[48] C.X. Ma, J.C. White, O.P. Dhankher, B.S. Xing, Metal-based Nanotoxicity and detoxification pathways in higher plants, Environ. Sci. Technol. 49 (12) (2015) 7109.

[49] T.R. Tavanti, A.A.R.D. Melo, L.D.K. Moreira, D.E.J. Sanchez, R.D. Silva, R.M. D. Silva, A.R.D. Reis, Micronutrient fertilization enhances ROS scavenging system for alleviation of abiotic stresses in plants, Plant Physiol. Biochem. 160 (2021) 386.

[50] B. Corsi, C. Forni, L. Riccioni, J.M.H. Linthorst, Enhancement of PR1 and PR5 gene expressions by chitosan treatment in kiwifruit plants inoculated with *Pseudomonas syringae* pv. Actinidiae, Eur. J. Plant Pathol. 147 (2) (2017) 471.

[51] Z. Michalkova, D. Martinez-Fernandez, M. Komarek, Interactions of two novel stabilizing amendments with sunflower plants grown in a contaminated soil, Chemosphere 186 (2017) 374.

[52] W. Xu, K.H. Cui, A.H. Xu, L.X. Nie, J.L. Huang, S.B. Peng, Drought stress condition increases root to shoot ratio via alteration of carbohydrate partitioning and enzymatic activity in rice seedlings, Acta Physiol. Plant. 37 (2) (2015) 9.

[53] B.Y. Yang, X.B. Li, L.W. Wu, Y.Y. Chen, F.L. Zhong, Y.S. Liu, F. Zhao, D.P. Ye, H. Y. Weng, *Citrus* Huanglongbing detection and semi-quantification of the carbohydrate concentration based on micro-FTIR spectroscopy, Anal. Bioanal. Chem. 414 (23) (2022) 6881.

[54] R. Berni, M. Luyckx, X. Xu, S. Legay, K. Sergeant, J.F. Hausman, S. Lutts, G. Cai, G. Guerriero, Reactive oxygen species and heavy metal stress in plants: impact on the cell wall and secondary metabolism, Environ. Exp. Bot. 161 (2019) 98.

[55] M. Ali, A. Parveen, Z. Malik, M. Kamran, M.H. Saleem, G.H. Abbasi, I. Ahmad, S. Ahmad, M. Sathish, M.K. Okla, S.S. Al-Amri, I.A. Alaraidh, S. Ali, Zn alleviated salt toxicity in *Solanum lycopersicum* L. seedlings by reducing $Na^+$ transfer, improving gas exchange, defense system and Zn contents, Plant Physiol. Biochem. 186 (2022) 52.

[56] Y.D. Li, Q. Jin, D.S. Yang, J.H. Cui, Molybdenum sulfide induce growth enhancement effect of rice (*Oryza sativa* L.) through regulating the synthesis of chlorophyll and the expression of aquaporin gene, J. Agric. Food Chem. 66 (16) (2018) 4013.

[57] M.S. Li, P. Zhang, Z.L. Guo, W.D. Cao, L. Gao, Y.B. Li, C.F. Tian, Q. Chen, Y.Z. Shen, F.Z. Ren, Y.K. Rui, J.C. White, I. Lynch, Molybdenum nanofertilizer boosts biological nitrogen fixation and yield of soybean through delaying nodule senescence and nutrition enhancement, ACS Nano 17 (15) (2023) 14761.

[58] P.J. Curran, J.L. Dungan, H.L. Gholz, Exploring the relationship between reflectance red edge and chlorophyll content in slash pine, Tree Physiol. 7 (1–4) (1990) 33.

[59] J.H. Yang, Z.Y. Song, J. Ma, H.Y. Han, Toxicity of molybdenum-based nanomaterials on the soybean- rhizobia symbiotic system: implications for nutrition, ACS Appl. Nano Mater. 3 (6) (2020) 5773.